Numerical modeling of p-i-n GaAs solar cell performance

E. Chahid[d,f,*], M. Nachaoui[b], Y. Mir[a], A. Amine[a,c], M.A. Kinani[a], A. Elrharib[a],
R. Abdia[c], A. Koumina[e], A. Malaoui[d], M. Zazoui[a]
[a]Laboratory of Materials, Energy and Control, Faculty of Sciences and Technology, University Hassan II of Casablanca, BP 146 Boulevard Hassan II, 20650 Mohammedia, Morocco
[b]Equipe de mathématiques & interactions (EMI), FST Béni-Mellal, université Sultan Moulay Slimane, Maroc
[c]Laboratory Instrumentation Measurements and Control, University Chouaib Doukkali, El Jadida, Morocco
[d]Resaerch Laboratory in Physicas and Sciences for Engineers (LRPSI), Polydisciplinary Faculty, Sultan Moulay Slimane University, Beni Mellal, Morocco
[e]Laboratoire Interdisciplinaire de Recherche en Bio-Ressources, Environnement et Matériaux, Ecole Normale Supérieure, Marrakech, Maroc
[f]Equipe Innovation en Métiers d'Enseignement et de Formation, Expérimentation et Orientation en Sciences, CRMEF, Beni Mellal, Maroc

This study aims to improve and evaluate the external quantum efficiency (EQE) of p-i-n GaAs solar cells. The current densities of minority carriers and the geometrical and physical cell parameters were calculated using the finite difference method. As a result, the EQE simulation findings are extremely close to the experimental data, and a maximum EQE of 57.26 %, with optimum layer thicknesses (μm) of p, i, and n are respectively 0.2,1,4, and n and p layers doping (cm^{-3}) of 10^{20} cm^{-3} and 4×10^{17} cm^{-3}. The adding of p+-AlGaAs window layer increases the energy conversion efficiency (%) from 19.41 to 25.45.

1. Introduction

Gallium Arsenide (GaAs) semiconductors are the most promising absorber materials in second-generation thin-film solar cells, with conversion efficiencies better than any silicon-based counterparts. During the last few years, the best (GaAs) laboratory solar cell has improved its conversion efficiency by 1.8 percent, from 26.2% in 2012 [1-4] to 29.3 % in 2021 [5,6]. GaAs solar cells are useful because of its Eg=1.425 eV direct band gap, which makes them appropriate for diode and photovoltaic (PV) cell applications. It is frequently expanded by alloying, which is the exact fusing of two components together, in this case aluminum, to produce $Al_xGa_{1-x}As$. A wide bandgap also indicates the material remains more semiconductive at higher temperatures, as in silicon that has a bandgap of 1.12 eV. As a result, the thermal generation of carriers becomes more dominant over the purposefully doped amount of carriers at higher temperatures [7- 9]. The performance of GaAs solar cells has been improved using a technique that focuses on improving their architectures, such as textured surfaces for light trapping and surface passivation, such as the SiO_2/Si interface to reduce surface recombination rate, and the use of an *AlGaAs* window and a back surface layer (BSF) to reduce surface recombination velocity

[10-13]. The p-i-n junction, which is made up of two layers of p and n regions with an intrinsic layer in the center, is another type of solar cell structure. Based on the width of the intrinsic region and the creation of an internal electric field that moves minority carriers away from the surface, this structure provides a straightforward strategy to enhance absorption capacity [14, 15]. The Layer window plays a significant role in improving the solar cell's performance. Unlike Silicon, they serve to reduce effective surface to surface recombination of the solar cell issuer without absorbing the beneficial light required for the device. On the basis of semiconductors made out of solar cells, many materials for the window layer have been investigated for III-V [16]. It has been proven with efficiency of 25% at one sun illumination in the case of GaAs solar cells, and high efficiency $Ga\,As$ solar cells all use a wide band-gap window layer on the surface to reduce front surface recombination losses. The $Al_xGa_{(1-x)}As$ window layer is one of the more crucial design areas in high efficiency $GaAs$ solar cells, and high aluminum content alloys are preferred to decrease optical absorption [17, 18]. Using the finite difference method, our model gives a numerical description of a $p - i - n$ solar cell structure. The numerical resolution of the continuity equations for minority carriers in each zone is used to calculate the current densities. This method is based on Thomas's algorithm, which is special to the resolution of tridiagonal matrix [19- 21]. In this study, The main goal is to first simulate a homojunction $GaAs$ solar cell using the finite difference method in order to evaluate photoelectric parameters (photocurrent density, doping levels of the emitter and base layers), geometrics (thickness of different regions), and then to improve solar cell efficiency by using $Al_xGa_{(1-x)}As$ ($x = 0.8$) type material as a window layer.

2. p-i-n GaAs solar cell structure

A diagram of the p-i-n solar cell structure based on the GaAs is illustrated in Fig.1, and the employed physical parameters in the numerical simulation are listed in Table 1. This structure is made up of a non-doped intrinsic region i-GaAs intercalated between two different areas, one of which is n-GaAs and the other is p-GaAs. The p-i-n structure provides an electric field between the p and n regions, which separates electron-hole pairs and prevents their recombination. Furthermore, electrons are excited from the valence band to the conduction band during light absorption, resulting holes in the valence band. The charge carrier types move through the material and contribute to the photocurrent production. The present structure was examined utilizing the Standard Conditions Test (STC), which includes an AM0 solar spectrum with constant light intensities of 100 mW/cm^2 and a cell temperature of 25°C.
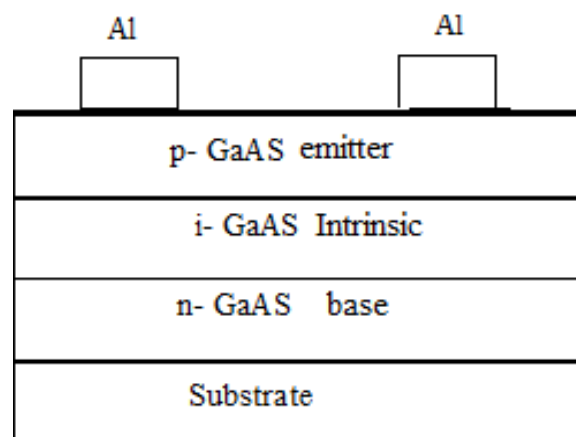

Fig. 1. Schematic diagram of single p-i-n GaAs solar cell.

Table 1. Geometric and physical parameters set for simulation of the p-i-n GaAs solar cell.

Parameters	Emitter	Intrinsic	Base
Thickness (nm)	200	100	200
Acceptor doping density $N_a(cm^{-3})$	5×10^{11}	--	--
Donor doping density $N_d(cm^{-3})$	----	----	5×10^{11}
Intrinsic Doping Density $N_i(cm^{-3})$	----	2.1×10^6	----
Mobility $(cm^2.V^{-1}.s^{-1})$	$\mu_p = 400$	---------	$\mu_n = 8500$
Recombination velocity (cm/s)	$S_p = 1 \times 10^6$	---------	$S_n = 5 \times 10^4$

3. Numerical simulation

A diagram of p-i-n GaAs solar cell structure used in the numerical simulation is illustrated in Fig. 2.
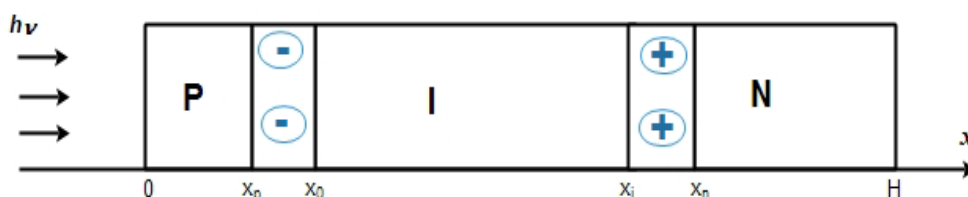

Fig. 2. Schematic structure of a p-i-n solar cell structure.

Minority carrier continuity equations in the p-region, i-region, and n-region are formulated as follows in the permanent regime:

$$\frac{1}{q}\frac{dJ_n}{dx} + G(x) - R_n(x) = 0 \tag{1}$$

$$\frac{1}{q}\frac{dJ_m}{dx} + G(x) = 0 \quad (m = n, m = p) \tag{2}$$

$$-\frac{1}{q}\frac{dJ_p}{dx} + G(x) - R_p(x) = 0 \tag{3}$$

where, R_n and R_p are the electrons and holes recombination rates, respectively. They are described in terms of excess concentration minority carriers (Δn for electrons, Δp for holes) relative to the dark equilibrium state (n_0, p_0). Their expression are respectively: $R_n = \frac{\Delta n}{\tau_n} = \frac{n-n_0}{\tau_n}$, $R_p = \frac{\Delta p}{\tau_p} = \frac{p-p_0}{\tau_p}$. The lifetimes of electrons and holes are indicated by the symbols τ_n and τ_p, respectively. The minority carriers concentrations (electrons and holes) in the p- and n- regions, at equilibrium are n_0, p_0 respectively. The generation rate $g(x,\lambda)$ for a given wavelength λ is calculated using the incident flux photons $\phi(x,\lambda)$, the absorption coefficient $\alpha(x,\lambda)$, and the reflexion coefficient losses R(x,) as follows: $g(x,\lambda) = (1 - R)\phi\alpha e^{-\alpha x}$. The total photocurrent density J_{ph} is the sum of the three components in each region; the drift current density of the

electrons in the *p-type* region J_n, the drift current density of the photoholes in the *n-type* region J_p, and the photogeneration in the intrinsic region J_i.

$$J_{ph}(\lambda) = J_n(\lambda) + J_i(\lambda) + J_p(\lambda) \tag{4}$$

where J_n , J_p are given by the following equations:

$$J_n(\lambda) = qn\mu_n E_p(x_p) + qD_n \frac{\partial n(x)}{\partial x} \tag{5}$$

$$J_p(\lambda) = qp\mu_p E_n(x_n) - qD_p \frac{\partial p(x)}{\partial x} \tag{6}$$

where μ_n, μ_p are the electron and hole mobility, and D_n, D_p are the electron and hole diffusion coefficients respectively. E_p, E_n are the electric field in the p-region and n-region, as determined by the poisson's equation:

$$\frac{dE}{dx} = \frac{\rho(x)}{\varepsilon} \tag{7}$$

where: ρ is the charge density in the three regions which is expressed as follows:

$$\rho(x) = \begin{cases} -eN_a, for\ x_p \leq x \leq x_0 \\ en_i = |ep_i|, for\ x_0 \leq x \leq x_i \\ eN_d\ , for\ x_i \leq x \leq x_n \\ 0,\ for\ x < x_p\ and\ x > x_n \end{cases} \tag{8}$$

By solving the Gauss equation (7), the electric field in the p-region, i-intrinsic, and n-region is obtained:

$$E(x) = \begin{cases} -\frac{eN_a}{\varepsilon}(x - x_p), for\ x_p \leq x \leq x_0 \\ -\frac{en_i}{\varepsilon}(x_i - x_0), for\ x_0 \leq x \leq x_i \\ \frac{eN_d}{\varepsilon}(x - x_n)\ , for\ x_i \leq x \leq x_n \end{cases} \tag{9}$$

The continuity equation for electrons density n(x) in the emitter region $(0 < x < x_p)$ takes the following form:

$$D_n \frac{\partial^2 n(x)}{\partial x^2} + \mu_n E(x) \frac{\partial n(x)}{\partial x} + n\mu_n \frac{\partial E(x)}{\partial x} + g_n - r_n = 0 \tag{10}$$

This equation is stated in the form of a 2nd order differential equation with a second member that is depending on x:

$$\frac{\partial^2 n(x)}{\partial x^2} - A_1(x) \frac{\partial n(x)}{\partial x} - B_1(x)n(x) = D(x) \tag{11}$$

where, $A_1(x) = \frac{\mu_n}{D_n}\frac{qN_a}{\varepsilon}(x - x_p); B_1(x) = \frac{\mu_n}{D_n}\frac{qN_a}{\varepsilon} + \frac{1}{L_n^2}; D(x) = -\frac{\phi_0\alpha(1-R)e^{-\alpha x}}{D_n} - \frac{n_i^2}{L_n^2 N_a}.$

The continuity equation for the generated excess holes density p(x) in the base region $(x_n < x < H)$ is treated similarly; it may be obtained by substituting only $'n'$ in the equation (14) with $'p'$. We neglect the recombination coefficient $'R'$ in the intrinsic region ($x_0 < x < x_i$), hence the photogeneration current density in this region is given as:

$$J_i(\lambda) = J_{in}(\lambda) + J_{ip}(\lambda) \tag{12}$$

where the current density of the minority carriers (electrons, holes) [22, 23] are written as bellow:

For electrons:
$$J_{in}(\lambda) = qn\mu_n E_i(x_p) + qD_n \frac{\partial n(x)}{\partial x} \qquad (13)$$

For holes:
$$J_{ip}(\lambda) = qpE_i(x_n) - qD_p \frac{\partial p(x)}{\partial x} \qquad (14)$$

The concentration of the minority carrier m(x) is numerically determined by using finite difference scheme [24, 25] to solve continuity equations (11). This method consists to replace the derivatives of the differential operators of the functions involved in the PDE using Taylor formulas, so as to search an approximation solution of partial differential equations (PDE) at points which are distributed on a grid. We notice h unit interval $[a \ b]$ of solar cell region defined as $h = \frac{b-a}{k}$, the values of grid point x_i have the following expression $x_i = a + i \, h$ for $i = 0,1,2,\dots,N+1$ with $x_0 = a$ and $x_k = b$ and the carrier concentrations are noted by $u(x_i) = u_i$. The cell's limits conditions impose boundary conditions to determine PDE solutions, which are described by the continuity of both the current density at the front area's cell, characterizing by the surface recombination velocity S_n, and the minority electrons concentration at the end of the zone's length. The obtained system of differential equations can be written in a tridiagonal matrix which is solved using the Thomas's algorithm [26] , as given as:

$$A_i m_{i-1} + B_i \, m_i + C_i m_{i+1} = D(x_i); \quad i = 1,2,\dots N \qquad (15)$$

where $A_i, B_i, \ C_i$ and $D(x_i)$ are coefficients according to each region. The total photocurrent density J_{ph} of the chosen spectrum is expressed in the form:

$$J_{ph} = \int_{\lambda_{min}}^{\lambda_{max}} J_{ph}(\lambda) \, d\lambda. \qquad (16)$$

The characteristic current – voltage J(V) described the relationship between the output current density across the ideal cell and the voltage V, which is expressed as:

$$J(V) = J_{ph} - J_s \left(\exp\left(\frac{qV}{ak_B T} \right) - 1 \right) \qquad (17)$$

where J_s is the saturation current density of the $p - n$ junction, q is the charge of the electron, T is the cell temperature and a is an ideality factor and has a value typically between 1 and 2 . The saturation current is given in the following simple expression:

$$J_s = \frac{qn_i^2 D_p}{N_d L_p} \qquad (A.cm^{-2}) \qquad (18)$$

L_p, L_n are the length diffusions both of holes and electrons respectively.

4. External quantum efficiency EQE and window layer

4.1. External quantum efficiency EQE

The external quantum efficiency EQE is defined as the ratio of the number of the produced electrons N_e collected by the solar cell to the number of the absorbed incident photons; The expression of EQE is given as a function of wavelength λ, as follows:

$$EQE(\lambda) = \frac{N_e}{N_v} \qquad (19)$$

This parameter is used to evaluate the photocurrent J_{ph} produced by a solar cell; this is done by integrating the EQE obtained over the entire spectrum of light radiation. This efficiency is directly related to the photon energy E_{ph}, incident flux $\varphi(\lambda)$, and photocurrent J_{ph}. It can be approximated as:

$$EQE(\lambda) = \frac{J_{ph}(\lambda).E_{ph}(\lambda)}{\varphi(\lambda).q} = 1.24 \times \frac{J_{ph}(\lambda)}{\lambda.\varphi(\lambda)} \tag{20}$$

4.2. Windows layer effect

Fig. 3 shows a schematic representation of the solar cell structure, and Table 2 lists the key physical parameters used in the simulations. As illustrated in Fig. 3, the basic structure for increasing solar cell performance is composed of a homojunction p-i-n-GaAs solar cell on which an $p^+ - Al_{0.8}Ga_{0.2}As$ type window layer is deposited to produce the heterojunction. The difference in lattice parameters between GaAs and $Al_xGa_{1-x}As$ ($0 \leq x \leq 1$) is relatively tiny (less than 0.15% percent at 300 K), particularly in the $Al_xGa_{1-x}As$ thin film material (in this study, x = 0.8 and band gap is about 2.09 eV because this usual x value of the window layer produces satisfactory results) [27]. Due to its indirect band gap, the $Al_xGa_{1-x}As$ window layer is visible to photons with energy up to roughly 2.1 eV and cuts off light gradually in the range 2.1-2.6 eV. This layer must not only allow for the reduction of recombination at the cell's front surface, but also make it more sensitive to photons with higher energy [28]. Table 2 shows the principal physical parameters used in the simulation [29].
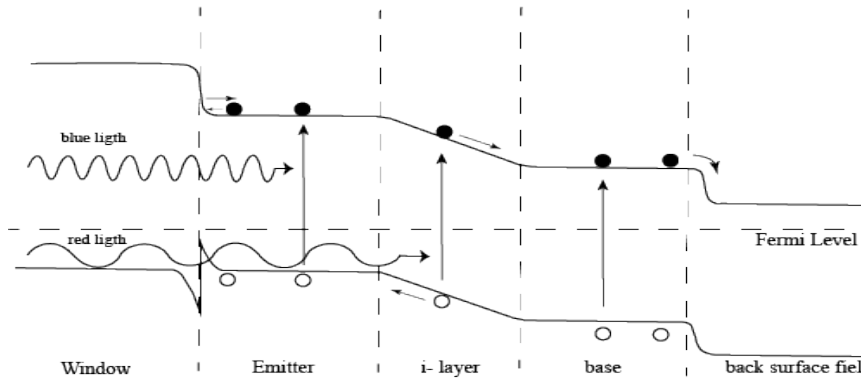

Fig. 3. band diagram of a photovoltaic cell p-n-GaAs in the presence of a normal p$^+$- AlGaAs window layer [18].

Table 2. Physical parameter values used in the simulation [30-31].

Material Parameters	$p^+ - Al_{0.8}Ga_{0.2}As$
Window thickness $X_W (\mu m)$	0.02
Band gap energy $E_g^W (eV)$	2.09
Diffusion coefficient $D_n^W (cm^2.s^{-1})$	4.6
Diffusion length $L_n^W (\mu m)$	0.5
Velocity recombination $S_n^W (cm.s^{-1})$	5×10^4
Window doping $N_A^W (cm^{-3})$	2×10^{18}

Insight into the mechanisms of recombination at the GaAs surface is necessary for precisely calculating the effect of the window layer. Indeed, solar cells made of GaAs and with a window of the type p$^+$- $Al_{0.8}Ga_{0.2}As$ (Fig. 2) reduce surface recombination, which is modeled using an effective surface recombination velocity S S_{eff}^n, which is expressed as [32]:

$$S_{eff}^n = S_n \exp\left(\frac{E_g - E_g^W}{K_b T}\right) \frac{\frac{D_n^W}{S_n^W L_n^W}\tanh\left(\frac{X_W}{L_n^W}\right)+1}{\frac{S_n^W L_n^W}{D_n^W}\tanh\left(\frac{X_W}{L_n^W}\right)+1} \tag{21}$$

5. Results and discussion

5.1. Electric field

In Fig.4 we represent the curve of the electric field depending on the thickness of the p-i-n GaAs solar cell. Due to the important absorption of the light, we note that the intermediary region delivers an important value of electric field. This curve demonstrates that the intrinsic region's insertion permits charge carriers to be generated, and so contributes to the increase in photogeneration current.
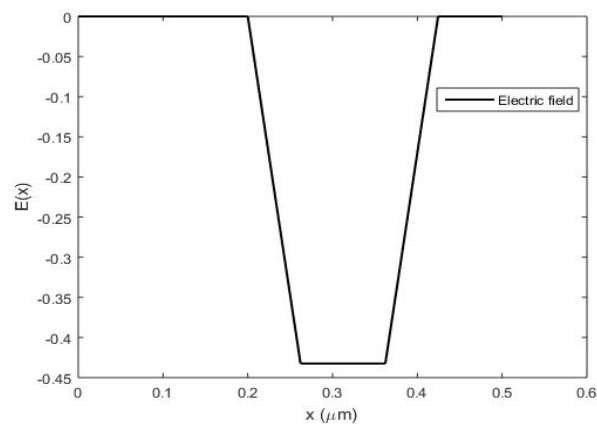

Fig. 4. Electric field of p-i-n GaAs solar cell.

5.2. External quantum efficiency EQE

The output characteristic variation of the external quantum efficiency (EQE) as a function of wavelength is shown in Fig. 4. The numerical simulation results of EQE correspond well with the experimental values, demonstrating the quality of our numerical method, which is the finite difference method. The optimum EQE values are found in the range of values between 300nm and 350nm. Furthermore, the EQE's maximum value is 57.26% and is located at 328.6 nm. The results demonstrate that this layer is significant in photovoltaic characteristics, especially during absorption. However, we note that the photo-carriers in the intrinsic region are involved in current generation.
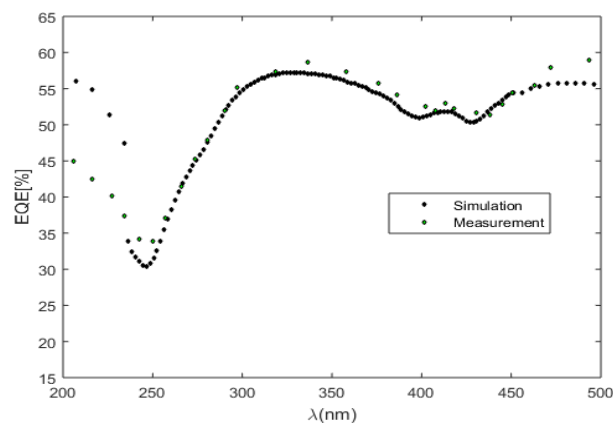

Fig. 5. Simulated EQE versus the wavelength of p-i-n GaAs solar cell.

5.3. Effect of the geometric parameters

Given the significance of various types of layers in photovoltaic properties, particularly during absorption phenomena. We have studied the effect of geometrical parameters such as the base and intrinsic layer thicknesses, as well as the additional physical parameters indicated in Table 1 are fixed, $X_E=0.2\mu m$, $N_A=4x10^{17}$ cm^{-3}.

5.3.1. Effect of the base layer thickness

In Fig. 6, we can see that as the base thickness grows, the short current density J_{sc} increases. Furthermore, the J_{sc} variation is proportional to the base thickness, and the variation increases rapid up to the optimal value $X_B = 4\mu m$ before stabilizing around a constant value.

5.3.2. Effect of the intrinsic layer thickness

The output characteristic of the cell's EQE is shown in Fig. 7 as a function of the intrinsic layer thickness W_i. As can be seen, the EQE improves when the intrinsic layer thickness is increased, which reaches a maximum of 57.26 % at $W_i = 0.1\mu m$. We concluded that the optimal geometric values are $X_B = 0.2\mu m$, $W = 1\mu m$, and $X_B = 4\mu m$, according to the results.
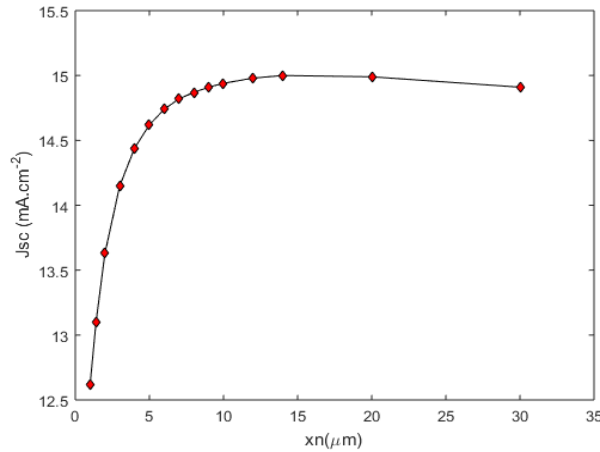

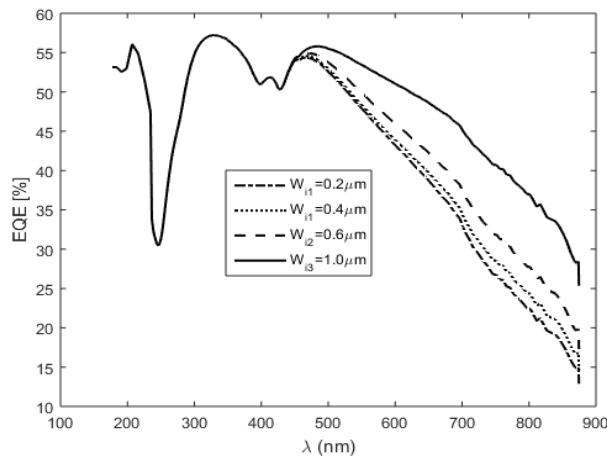*Fig. 6. Base thickness x_n Effect on J_{sc}.*

Fig. 7. $EQE(\lambda)$ characteristic variation as a function of wavelength.

5.4. Characteristic J(V) of a pin GaAs solar cell

With the previous geometric and physical values, as well as others in Table 1, are used. We represent the solar cell's characteristic J (V) based on p-i-n GaAs structure in Fig. 8 by using the finite difference method. It is can be seen that the characteristic solar cell's J(V) is "hand in hand" with literature results and follows the typical form of photoelectric cells.
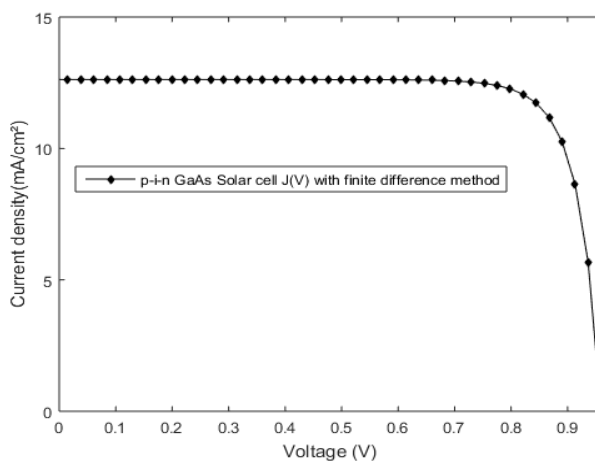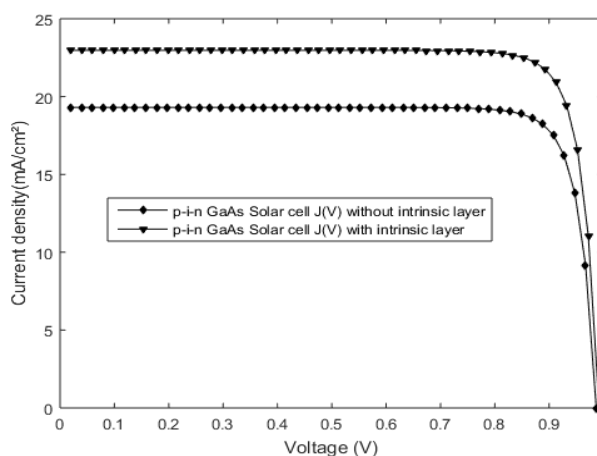

Fig. 8. p-i-n GaAs solar cell's J(V).

Fig. 9. p-i-n GaAs solar cell's J(V) with and without intrinsic layer .

On the other hand, to investigate the impact of the intrinsic layer on energy conversion efficiency, we compare the J(V) characteristic with and without the intrinsic layer. Fig. 9 indicates that the short circuit current J_{sc} is increased from 19.41 mA/cm^2 to 24.45 mA/cm^2, while the voltage V_{oc} remains constant at 0.9995 V, and subsequently the energy conversion efficiency η is increased.

5.5. Window layer effect on solar cell's J(V)

To determine the importance of the window layer in the GaAs solar cell, we have carried a comparative study between two cells; the first one is with window and the second one without window layer. Fig. 10 shows the p-i-n GaAs solar cell's J(V) with and without $Al_{0.8}Ga_{0.2}As$ window layer type. It can be seen, that adding a window layer increases the short-circuit current while keeping V_{oc} unchanged. Indeed, the $p^+-Al_{0.8}Ga_{0.2}As/\ p-GaAs$ heterostructure junction reduces the velocity recombination S_n in response to the difference in band gap energy of the two

materials, forming a potential barrier that inhibits minority carriers from crossing it and contributing to photocurrent production.
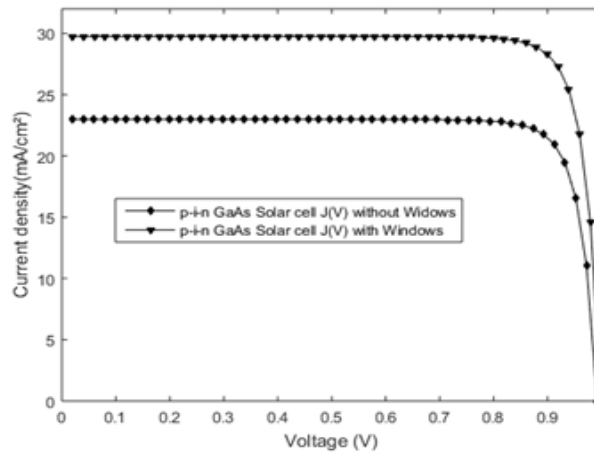

Fig. 10. $p^+ - Ga_{0.2}Al_{0.8}As$ window Effect on the solar cell's J(V).

Table 3 shows the photovoltaic parameter values for the two cells. By adding a window layer $Al_{0.8}Ga_{0.2}As$ type, the photocurrent increased from 22.97 to 25.75 mA/cm^2 and the energy conversion efficiency η increased from 19.41 %to 25.45%.

Table 3. Simulated photovoltaic parameters of a p-i-n GaAs solar cell with and without window.

Photovoltaic parameters	cell without window	Cell with window
Jsc (mA/cm²)	22.97	25.75
V_{oc} (V)	0.9919	0.9995
η(%)	19.41	25.45

6. Conclusion

We have simulated the external quantum efficiency of $p - i - n\ GaAs$ solar cell, using the finite difference method. This model has permitted us to study the influence of intrinsic region cell on the photovoltaic performance covering all solar spectrum, and the effect of adding a $p^+ - Al_{0.8}Ga_{0.2}As$ window layer on the performance solar cell. The obtained results show an improvement in the performance cell when the wavelength is located between 300nm and 350 nm. EQE has a maximum value of 57.26 %, which is found at a wavelength of 328.6 nm. The comparison between simulation and experimental values are in good agreement, which is show the certitude and the accuracy of our numerical method. Furthermore, it demonstrates that both the intrinsic and window layers have a considerable impact on the performance of the $pn - GaAs$ solar cell; this leads to an increase in energy conversion efficiency, with the optimum value of 25.45 %.

References

[1] BM. Kayes, H. Nie, R. Twist, SG. Spruytte, F. Reinhardt, IC. Kizilyalli, GS. Higashi, Proceedings of the 37th IEEE Photovoltaic Specialists Conference, (2011).
[2] LS. Mattos, SR. Scully, M. Syfu, et al, Proceedings of the 38th IEEE Photovoltaic Specialists Conference, (2012).
[3] M. A. Green, K. Emery, Y. Hishikawa, W. Warta and E. D. Dunlop, Progress Photovoltaics: Research and Applications 24, 905 (2016); https://doi.org/10.1002/pip.2788
[4] E. Chahid, M. I. Oumhanad, M. Feddaoui,A. Malaoui, Journal of Ovonic Research 13 (3), 119

(2017).

[5] M. A. Green, E. D. Dunlop, J. Hohl-Ebinger, M. Yoshita, N. Kopidakis, X. Hao, Progress Photovoltaics Research and Applications 28, 628 (2020); https://doi.org/10.1002/pip.3303

[6] G S.Kinsey, Solar Energy 217, 49-57, (2021); https://doi.org/10.1016/j.solener.2021.01.024

[7] A.R. Barron, Chemistry of Electronic Materials; Midas Green Innovations: Swansea, Wales, 214 (2021).

[8] P. Arickx, R. Kurstjens, W. Geens K. Dessein, E3S Web 16, 03010 (2017); https://doi.org/10.1051/e3sconf/20171603010

[9] M.A. Kinani, R. Chami, A. Lekdadri, A. ElRharib, Y. Mir, E.K. Hlil, A. Amine, M. Zazoui, Computational Condensed Matter 26,520 (2020).

[10] N. Papež, Degradation of GaAs Solar Cells, Ph.D. Thesis, Brno University of Technology, Brno, Czech Republic, 2021.

[11] H. Bourbaba, S. Kadri, and K. Djermane, Journal of Ovonic Research 15 (3),151 (2019).

[12] A. Suhandi, Y. R. Tayubi, A. Samsudin, International Journal of Scientific & Technology Research 9(4), (2020).

[13] Z. Li, Y.C. Wenas,L. Fu, S. Mokkapati, H.H. Tan, C. Jagadish, IEEE J Photovoltaics 5(3), 854 (2015); https://doi.org/10.1109/JPHOTOV.2015.2405753

[14] Y. Wu, X. Yan, W. Wei et al, Nanoscale Research Letters, 13, 126 (2018); https://doi.org/10.1186/s11671-018-2503-8

[15] D. Khatiwada D, CA. Favela, S. Sun et al, Progress in Photovoltaics: Research and Applications 11, 1107(2020); https://doi.org/10.1002/pip.3308

[16] H. Fujii, K. Toprasertpong, H. Sodabanlu, K. Watanabe, M. Sugiyama, Y. Nakano, Journal of Applied Physics 116, 203101 (2014); https://doi.org/10.1063/1.4902319

[17] A.F. Meftah, N. Sengouga, A.M. Meftah, S. Khelifi, Renewable Energy 34, 2426 (2009); https://doi.org/10.1016/j.renene.2009.03.013

[18] Y. Mir, A. Amine, M. Bouabdellaoui, K. Zazi, and M. Zazoui, Optical and Quantum Electroncs, vol. 45, 1189-1197 (2013); https://doi.org/10.1007/s11082-013-9735-8

[19] R. Belghouthi, J. P. Salvestrini, M. H. Gazzeh, and C. Chevallier, Superlattices and Microstructures, 100, 168 (2016); https://doi.org/10.1016/j.spmi.2016.09.016

[20] B. Chouchen , M. H. Gazzah , A. Bajahzar, and H. Belmabrouk, AIP Advances 9, 045313 (2019); https://doi.org/10.1063/1.5092236

[21] N. Ben Afkir, F. Dujardin, M. Zazoui, and J. Meziane, Physica B: Physics of Condensed Matter 534, 10 (2018); https://doi.org/10.1016/j.physb.2018.01.005

[22] H. Mathieu, Physique des semi-conducteurs et des composants électroniques, Edition Masson, Paris, 1990.

[23] H. J. Hovel, Semicondutors and Semimetals , New York:Academic, vol 11, 1979.

[24] M. Boumahrat et A. Gourdin, Méthodes Numériques Appliquées, OPU, 1993.

[25] J. P. Nougier, Méthodes de calcul numérique, Hermes science publications, ISBN 2-7462-0279-4, Paris, 2001.

[26] WH. Press, WT. Vettering and SA. Teukolsky, Numerical Recipes in C: the Art of Scientific Computing, 2nd Ed. Cambridge University Press, Vol. 9, pp. 362 - 367, 2002.

[27] S. Adachi, Journal of Applied Physics, 58(3), R1-29, (1985); https://doi.org/10.1063/1.336070

[28] S. Adachi, Properties of aluminium gallium arsenide, Institution of Engineering & Technology, 1993.

[29] M. Levinshtein, M. Shur, Handbook Series on Semiconductor Parameters: ternary and quaternary III-V compounds, 1996; https://doi.org/10.1142/2046-vol2

[30] E. Grunbaumt,E. Napchanll,Z. Barkayy, et al, Semicond. Sci.Technol 10, 627 (1995).

[31] J. Nelson, The physics of solar cells properties of semiconductor materials, 1 edition, imperial college press, 2003.

[32] A. Amine, M. Bouabdellaoui, K. Zaz, Y. Mir, M. Zazoui, Smart Grid and Renewable Energy 8, 46-51, (2017); https://doi.org/10.4236/sgre.2017.81003